

An unsupervised algorithm for learning Lie group transformations

Jascha Sohl-Dickstein^{1, 4, 5}

Ching Ming Wang^{1, 2, 6}

Bruno Olshausen^{1, 2, 3}

¹Redwood Center for Theoretical Neuroscience, ²School of Optometry, ³Helen Wills Neuroscience Institute, University of California, Berkeley.

⁴Department of Applied Physics, Stanford University.

⁵Khan Academy.

⁶earthmine inc.

Keywords: Lie group, video coding, transformation, natural scene statistics, dynamical systems

Abstract

We present several theoretical contributions which allow Lie groups to be fit to high dimensional datasets. Transformation operators are represented in their eigen-basis, reducing the computational complexity of parameter estimation to that of training a linear transformation model. A transformation specific “blurring” operator is introduced that allows inference to escape local minima via a smoothing of the transformation space. A penalty on traversed manifold distance is added which encourages the discovery of sparse, minimal distance, transformations between states. Both learning and inference are demonstrated using these methods for the full set of affine transformations on natural image patches. Transformation operators are then trained on natural video sequences.

It is shown that the learned video transformations provide a better description of inter-frame differences than the standard motion model based on rigid translation.

1 Introduction

Over the past several decades, research in the natural scene statistics community has shown that it is possible to learn efficient representations of sensory data, such as images and sound, from their intrinsic statistical structure. Such representations exhibit higher coding efficiency as compared to standard Fourier or wavelet bases [Lewicki and Olshausen, 1999], and they also match the neural representations found in visual and auditory systems [Olshausen and Field, 1996, van Hateren and van der Schaaf, 1998, Smith and Lewicki, 2006]. Here we explore whether such an approach may be used to learn *transformations* in data by observing how patterns change over time, and we apply this to the problem of coding image sequences, or video.

A central problem in video coding is to find representations of image sequences that efficiently capture how image content changes over time. Current approaches to this problem are largely based on the assumption that local image regions undergo a rigid spatial translation from one frame to the next, and they encode the local motion along with the resulting prediction error [Wiegand et al., 2003]. However, the spatiotemporal structure occurring in natural image sequences can be quite complex due to occlusions, the motion of non-rigid objects, lighting and shading changes, and the projection of 3D motion onto the 2D image plane. Attempting to capture such complexities with a simple translation model leads to larger prediction errors and thus a higher bit rate. The right approach would seem to require a more complex transformation model that is adapted to the statistics of how images actually change over time.

The approach we propose here is based on learning a Lie (continuous transformation) group representation of the dynamics which occur in the visual world [Rao and Ruderman, 1999, Miao and Rao, 2007, Culpepper and Olshausen, 2010, Cohen and Welling, 2014]. The Lie group is built by first describing each of the infinitesimal transformations which an image may undergo. The full group is then generated from all possible compositions of those infinitesimal transformations, which allows for transformations to be applied smoothly and continuously. A large class of visual transfor-

mations, including all the affine transformations, intensity changes due to changes in lighting, and contrast changes can be described simply using Lie group operators. Spatially localized versions of the preceding transformations can also be captured. In [Miao and Rao, 2007, Rao and Ruderman, 1999], Lie group operators were trained on image sequences containing a subset of affine transformations. [Memisevic and Hinton, 2010] trained a second order restricted Boltzmann machine on pairs of frames, an alternative technique which also shows promise for capturing temporal structure in video.

Despite the simplicity and power of the Lie group representation, training such a model is difficult, in part due to the high computational cost of evaluating and propagating learning gradients through matrix exponentials. Previous work [Rao and Ruderman, 1999, Miao and Rao, 2007, Olshausen et al., 2007] has approximated the full model using a first order Taylor expansion, reducing the exponential model to a linear one. While computationally efficient, a linear model approximates the full exponential model only for a small range of transformations. This can be a hinderance in dealing with real video data, which can contain large changes between pairs of frames. Note that in [Miao and Rao, 2007], while the full Lie group model is used in inferring transformation coefficients, only its linear approximation is used during learning. [Culpepper and Olshausen, 2010] work with a full exponential model, but that technique requires performing a costly eigendecomposition of the effective transformation operator for each sample and at every learning or inference step.

Another hurdle one encounters in using a lie group model to describe transformations is that the inference process, which computes the transformation between a pair of images, is highly non-convex with many local minima. This problem has been extensively studied in image registration, stereo matching and the computation of optic flow. For a specific set of transformations (translation, rotation and isotropic scaling), [Kokiopoulou and Frossard, 2009] showed that one could find the global minimum by formulating the problem using an overcomplete image representation composed of Gabor and Gaussian basis functions. For arbitrary transformations, one solution is to initialize inference with many different coefficient values [Miao and Rao, 2007]; but the drawback here is that the number of initial guesses grows exponentially with the number of transformations. Alternatively, [Lucas and Kanade, 1981, Vasconcelos and Lippman, 1997, Black and Jepson, 1996] perform matching with an image pyramid,

using solutions from a lower resolution level to seed the search algorithm at a higher resolution level. [Culpepper and Olshausen, 2010] used the same technique to perform learning with Lie Group operators on natural movies. Such piecewise coarse-to-fine schemes avoid local minima by searching in the smooth parts of the transformation space before proceeding to less smooth parts of the space. This constitutes an indirect method of coarsening the transformation through spatial blurring. As we show here, it is also possible to smooth the transformation space directly, resulting in a robust method for estimating transformation coefficients for arbitrary transformations.

In this work we propose a method for directly learning the Lie group operators that mediate continuous transformations in natural movies, and we demonstrate the ability to robustly infer transformations between frames of video using the learned operators. The computational complexity of learning the operators is reduced by re-parametrizing them in terms of their eigenvectors and eigenvalues, resulting in a complexity equivalent to that of the linear approximation. Inference is made robust and tractable by smoothing the transformation space directly, which allows for a continuous coarse-to-fine search for the transformation coefficients. Both learning and inference are demonstrated on test data containing a full set of known affine transformations. The same technique is then used to learn a set of Lie operators describing changes between frames in natural movies, where the optimal solution is not known. Unlike previous Lie group implementations, we demonstrate an ability to work simultaneously with multiple transformations and large inter-frame differences during both inference and learning. In another paper we additionally show the utility of this approach for video compression [Wang et al., 2011].

2 Model

As in [Rao and Ruderman, 1999], we consider the class of continuous transformations described by the first order differential equation

$$\frac{\partial \mathbf{x}(\mu)}{\partial \mu} = \mathbf{A} \mathbf{x}(\mu), \quad (1)$$

where $\mathbf{x}(\mu) \in \mathcal{R}^{N \times 1}$ represents the pixel values in a $\sqrt{N} \times \sqrt{N}$ image patch, $\mathbf{A} \in \mathcal{R}^{N \times N}$ is an infinitesimal transformation operator and the generator of the Lie group,

and $\mathbf{x}(\mu) \in \mathcal{R}^{N \times 1}$ is the image $\mathbf{x}(0)$ transformed by \mathbf{A} by an amount $\mu \in \mathcal{R}$. This differential equation has solution

$$\mathbf{x}(\mu) = e^{\mathbf{A}\mu} \mathbf{x}(0) = T(\mu) \mathbf{x}(0). \quad (2)$$

$T(\mu) = e^{\mathbf{A}\mu}$ is a matrix exponential defined by its Taylor expansion.

Our goal is to use transformations of this form to model the changes between adjacent frames $\mathbf{x}^{(t)}, \mathbf{x}^{(t+1)} \in \mathcal{R}^{N \times 1}$ that occur in natural video. That is, we seek to find the model parameters A (adapted over an ensemble of video image sequences) and coefficients $\mu^{(t)}$ (inferred for each pair of frames) that minimize the reconstruction error

$$E = \sum_t \|\mathbf{x}^{(t+1)} - T(\mu^{(t)}) \mathbf{x}^{(t)}\|_2^2. \quad (3)$$

This will be extended to multiple transformations below.

2.1 Eigen-decomposition

To derive a learning rule for \mathbf{A} , it is necessary to compute the gradient $\frac{\partial e^{\mathbf{A}\mu}}{\partial \mathbf{A}}$. Under naive application of the chain rule this requires $O(N^6)$ operations [Ortiz et al., 2001] ($O(N^2)$ operations per element $\times N^4$ elements), making it computationally intractable for many problems of interest. However, this computation reduces to $\approx O(N^2.4)$ (the complexity of matrix inversion) if A is rewritten in terms of its eigen-decomposition, $\mathbf{A} = \mathbf{U}\mathbf{\Lambda}\mathbf{U}^{-1}$, and learning is instead performed directly in terms of \mathbf{U} and $\mathbf{\Lambda}$. $\mathbf{U} \in \mathcal{C}^{N \times N}$ is a complex matrix consisting of the eigenvectors of \mathbf{A} , $\mathbf{\Lambda} \in \mathcal{C}^{N \times N}$ is a complex diagonal matrix holding the eigenvalues of \mathbf{A} , and \mathbf{U}^{-1} is the inverse of \mathbf{U} . The matrices must be complex in order to facilitate periodic transformations, such as rotation. Note that \mathbf{U} need not be orthonormal. The benefit of this representation is that

$$e^{\mathbf{U}\mathbf{\Lambda}\mathbf{U}^{-1}\mu} = \mathbf{I} + \mathbf{U}\mathbf{\Lambda}\mathbf{U}^{-1}\mu + \frac{1}{2}\mathbf{U}\mathbf{\Lambda}\mathbf{U}^{-1}\mathbf{U}\mathbf{\Lambda}\mathbf{U}^{-1}\mu^2 + \dots = \mathbf{U}e^{\mu\mathbf{\Lambda}}\mathbf{U}^{-1} \quad (4)$$

where the matrix exponential of a diagonal matrix is simply the element-wise exponential of its diagonal entries. This representation therefore replaces the full matrix exponential by two matrix multiplications, a matrix inversion, and an element-wise exponential.

This change of form enforces the restriction that \mathbf{A} be diagonalizable. We do not expect this restriction to be onerous, since the set of non-diagonalizable matrices is

measure zero in the set of all matrices. However some specific desirable transformations may be lost. For instance, since nilpotent matrices are non-diagonalizable, translation without periodic boundary conditions (translation where content is lost as it moves out of frame) cannot be captured by this approach.

2.2 Adaptive Smoothing

In general the reconstruction error described by Equation 3 is highly non-convex in μ and contains many local minima. To illustrate, the red solid line in Figure 1 plots the reconstruction error for a white-noise image patch shifted by three pixels to the right as a function of transformation coefficient μ for a generator \mathbf{A} corresponding to left-right translation. It is clear that performing gradient descent-based inference on μ for this error function would be problematic.

To overcome this problem, we propose a multi-scale search that adaptively smooths the operator over a range of transformation coefficients. Specifically, the operator is averaged over a range of transformations using a Gaussian weighting for the coefficient values

$$T(\mu, \sigma) = \int_{-\infty}^{\infty} T(s) \frac{1}{\sqrt{2\pi}\sigma} e^{-\frac{(s-\mu)^2}{2\sigma^2}} ds \quad (5)$$

$$= \mathbf{U} \left[\int_{-\infty}^{\infty} e^{\Lambda s - \mathbf{I} \frac{(s-\mu)^2}{2\sigma^2}} \frac{1}{\sqrt{2\pi}\sigma} ds \right] \mathbf{U}^{-1} \quad (6)$$

$$= \mathbf{U} e^{\mu\Lambda} e^{\frac{1}{2}\Lambda^2\sigma^2} \mathbf{U}^{-1}. \quad (7)$$

$T(\mu, \sigma)$ replaces $T(\mu)$ in Equation 3. The error is then minimized with respect to both μ and σ .¹

Instead of finding the single best value of μ that minimizes E , $T(\mu, \sigma)$ allows for a Gaussian distribution over μ , effectively blurring the signal along the transformation direction given by $\mathbf{A} = \mathbf{U}\Lambda\mathbf{U}^{-1}$. In the case of translation, for instance, this averaging

¹This can alternatively be seen as introducing an additional transformation operator, this one a smoothing operator

$$\mathbf{A}_{smooth} = \frac{1}{2}\mathbf{U}\Lambda^2\mathbf{U}^{-1},$$

with coefficient $\mu_{smooth} = \sigma^2$. \mathbf{A}_{smooth} smooths along the transformation direction given by $\mathbf{A} = \mathbf{U}\Lambda\mathbf{U}^{-1}$.

over a range of transformations blurs the image along the direction of translation. The higher the value of σ , the larger the blur. This blurring is specific to the operator \mathbf{A} (e.g., if \mathbf{A} corresponded to rotation in one quadrant of an image patch, then this averaging would lead to rotational blur in that single quadrant). Under simultaneous inference in μ and σ , images are matched first at a coarse scale, and the match refines as the blurring of the image decreases. This approach is in the spirit of Arathorn’s map-seeking circuit [Arathorn, 2002], and also in the spirit of the transformation specific blurring kernels presented in [Mobahi et al., 2012]. [Mobahi et al., 2012] differs in that they fix the blurring coefficient σ rather than inferring it; in that their smoothing is specific to affine transformations and homography, while ours applies to all first order differential operators; and that they smooth the full objective function, rather than the transformation kernel.

To illustrate the way in which the proposed transformation leads to better inference, the dotted lines in Figure 1 shows the reconstruction error as a function of μ for different values of σ . Note that, by allowing σ to vary, steepest descent paths open out of the local minima, detouring through coarser scales.

2.3 Multiple Transformations

A single transformation is inadequate to describe most changes observed in the visual world. The model presented above can be extended to multiple transformations by concatenating transformations in the following way:

$$T_{\text{multi}}(\mu, \sigma) = T_1(\mu_1, \sigma_1) T_2(\mu_2, \sigma_2) \dots = \prod_k T_k(\mu_k, \sigma_k) \quad (8)$$

$$T_k(\mu_k, \sigma_k) = \mathbf{U}_k e^{\mu_k \mathbf{\Lambda}_k} e^{\frac{1}{2} \mathbf{\Lambda}_k^2 \sigma_k^2} \mathbf{U}_k^{-1} \quad (9)$$

where k indexes the transformation. Note that the transformations $T_k(\mu_k, \sigma_k)$ do not in general commute, and thus the ordering of the terms in the product must be maintained.

Because of the fixed ordering of transformations and due to the lack of commutativity, the multiple transformation case no longer constitutes a Lie group for most choices of transformation generators \mathbf{A} . Describing the group structure of this new model is a goal of future work. For the present, we note that many obvious video transformations – affine transformations, brightness scaling, and contrast scaling – can be fully

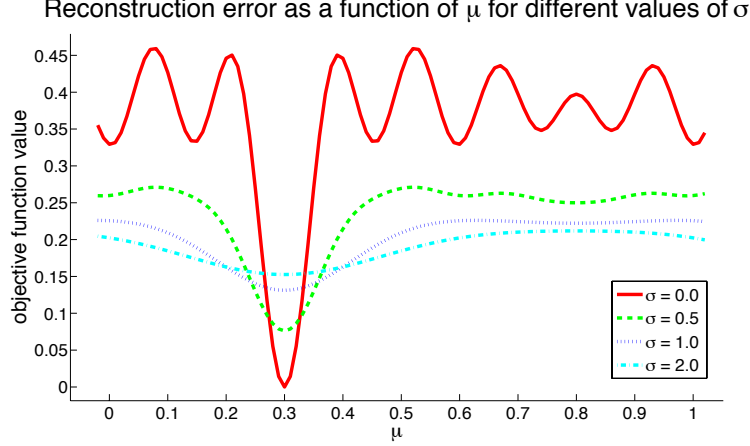


Figure 1: Local minima in the error function landscape can be escaped by increasing the smoothing coefficient σ . This plot shows reconstruction error (Equation 3) as a function of transformation coefficient μ for several values of the smoothing coefficient σ . In this case the target pattern $x^{(t+1)}$ has been translated in one dimension relative to an initial white noise pattern $x^{(t)}$, and the operator A is the one-dimensional translation operator.

captured by the model form in Equation 8, though the choice of coefficient values μ_k for a transformation may depend on the order of terms in the product.

2.4 Regularization via Manifold Distance

In order to encourage the learned operators to act independently of each other, and to learn to transform between patches in the most direct way possible, we penalize the distance through which the transformations move the image through pixel space. Since this penalty consists of a sum of the distances traversed by each operator, it acts similarly to an L1 penalty in sparse coding, and encourages travel between two points to occur via a path described by a single transformation, rather than by a longer path described by multiple transformations.

The distance traversed by the transformations can be expressed as

$$d_{\text{multi}} = \sum_k d_k(\mu_k, \mathbf{y}_k(0)) \quad (10)$$

where $\mathbf{y}_k(0) = \prod_{m < k} T_m(\mu_m, \sigma_m) \mathbf{x}(0)$ is the image patch prior to application of trans-

formation k . Assuming a Euclidean metric, and neglecting the effect of adaptive blurring, the distance $d_k(\mu_k, \mathbf{y}_k(0))$ traversed by each single transformation in the chain is

$$d_k(\mu_k, \mathbf{y}_k(0)) = \int_0^{\mu_k} \|\dot{\mathbf{y}}_k(\tau)\|_2 d\tau \quad (11)$$

$$= \int_0^{\mu_k} \|\mathbf{A}_k \mathbf{y}_k(\tau)\|_2 d\tau \quad (12)$$

$$= \int_0^{\mu_k} \|\mathbf{A}_k e^{\mathbf{A}_k \tau} \mathbf{y}_k(0)\|_2 d\tau \quad (13)$$

Finding a closed form solution for the above integral is difficult, but it can be approximated using a linearization around $\tau = \frac{\mu_k}{2}$,

$$d_k(\mu_k, \mathbf{y}_k(0)) \approx |\mu_k| \|\mathbf{A}_k e^{\mathbf{A}_k \frac{\mu_k}{2}} \mathbf{y}_k(0)\|_2^1. \quad (14)$$

2.5 The Complete Model

Putting together the components above, the full model's objective function is

$$\begin{aligned} E(\mu, \sigma, \mathbf{U}, \mathbf{\Lambda}, \mathbf{x}) = & \eta_n \sum_t \|\mathbf{x}^{(t+1)} - T_{multi}(\mu^{(t)}, \sigma^{(t)}) \mathbf{x}^{(t)}\|_2^2 \\ & + \eta_d \sum_t \sum_k \mu_k^{(t)} \|\mathbf{A}_k e^{\frac{\mu_k^{(t)}}{2} \mathbf{A}_k} \mathbf{x}_k^{(t)}\|_2^1 \\ & + \eta_\sigma \sum_t \sum_k (\sigma_k^{(t)})^2 \end{aligned} \quad (15)$$

A small L2 regularization term on $\sigma_k^{(t)}$ is included as it was found to speed convergence during learning. We used $\eta_n = 1$, $\eta_d = 0.005$, and $\eta_\sigma = 0.01$.

2.6 Inference and Learning

To find \mathbf{U} and $\mathbf{\Lambda}$, we use Expectation-Maximization with a MAP approximation to the expectation step. This iterates between the following two steps:

1. For a set of video patches \mathbf{x} , find optimal estimates for the latent variables $\hat{\mu}$ and $\hat{\sigma}$ for each pair of frames, while holding the estimates of the model parameters $\hat{\mathbf{U}}$ and $\hat{\mathbf{\Lambda}}$ fixed,

$$\hat{\mu}, \hat{\sigma} = \underset{\mu, \sigma}{\operatorname{argmin}} E(\mu, \sigma, \hat{\mathbf{U}}, \hat{\mathbf{\Lambda}}, \mathbf{x}). \quad (16)$$

2. Optimize the estimated model parameters $\hat{\mathbf{U}}$ and $\hat{\mathbf{\Lambda}}$ while holding the latent variables fixed,

$$\hat{\mathbf{U}}, \hat{\mathbf{\Lambda}} = \underset{\mathbf{U}, \mathbf{\Lambda}}{\operatorname{argmin}} E(\hat{\mu}, \hat{\sigma}, \mathbf{U}, \mathbf{\Lambda}, \mathbf{x}) \quad (17)$$

All optimization was performed using the L-BFGS implementation in minFunc [Schmidt, 2009].

Note that there is a degeneracy in \mathbf{U}_k , due to the fact that the columns (corresponding to the eigenvectors of \mathbf{A}_k) can be rescaled arbitrarily, and \mathbf{A}_k will remain unchanged as the inverse scaling will occur in the rows of \mathbf{U}_k^{-1} . If not dealt with, \mathbf{U}_k and/or \mathbf{U}_k^{-1} can random walk in column or row length over many learning steps, until one or both is ill conditioned. As described in detail in the appendix, this effect is compensated for by rescaling the columns of \mathbf{U}_k such that they have identical power to the corresponding rows in \mathbf{U}_k^{-1} . Similarly, there is a degeneracy in the relative scaling of μ and $\mathbf{\Lambda}$. In order to prevent $\hat{\mu}$ or $\hat{\mathbf{\Lambda}}$ from random walking to large values, after every iteration $\hat{\mu}_k$ is multiplied by a scalar α_k , and $\hat{\mathbf{\Lambda}}_k$ is divided by α_k , where α_k is chosen such that $\hat{\mu}_k$ has unit variance over the training set.

3 Experimental Results

3.1 Inference with Affine Transforms

To verify the correctness of the proposed inference algorithm a test dataset containing a set of known transformations was constructed by applying affine transformations to natural image patches. The transformation coefficients were then inferred using a set of pre-specified operators matching those used to construct the dataset. For this purpose a pool of 1000 11×11 natural image patches were cropped from a set of short video clips from The BBC’s *Animal World Series*. Each image patch was transformed by the full set of affine transformations simultaneously with the transformation coefficients drawn uniformly from the ranges listed below. ²

²Vertical skew is left out since it can be constructed using a combination of the other affine operators.

Transformation Type	Range
horizontal translation	± 5 pixels
vertical translation	± 5 pixels
rotation	± 180 degrees
horizontal scaling	± 50 %
vertical scaling	± 50 %
horizontal skew	± 50 %

The eigenvector matrices \mathbf{U}_k were initialized with isotropic unit norm zero mean Gaussian noise, followed by the transformation described in Appendix A. The eigenvalues Λ_k were initialized as $\Lambda_{kjj} = \tilde{n}_{\mathcal{I}}i + 0.01\tilde{n}_{\mathcal{R}}$, where Λ_{kjj} is the j th diagonal entry in eigenvalue matrix Λ_k , $\tilde{n}_{\mathcal{I}}$ and $\tilde{n}_{\mathcal{R}}$ are both unit norm zero mean Gaussians, and $i = \sqrt{-1}$. Finally, for each sample μ_k and σ_k were initialized as $\mu_k \sim \mathcal{N}(0, 10^{-4})$, $\sigma_k \sim \mathcal{N}(0, 0.04)$.

The proposed inference algorithm (Equation 16) is used to recover the transformation coefficients. Figure 2 shows the fraction of the recovered coefficients which differed by less than 1% from the true coefficients. The distribution of the PSNR of the reconstruction is also shown. The inference algorithm recovers the coefficients with a high degree of accuracy. The PSNR in the reconstructed images patches was higher than 25dB for 85% of the transformed image patches. In addition, we found that adaptive blurring significantly improved inference, as evident in Figure 2a.

3.2 Learning Affine Transformations

To demonstrate the ability to learn transformations, we trained the algorithm on image sequences transformed by a single affine transformation operator (translation, rotation, scaling, or skew). The training data used were single image patches from the same BBC clips as in Section 3.1, transformed by an open source Matlab package [Shen, 2008] with the same transformation range used in Section 3.1. Initialization was the same as in Section 3.1.

The affine transformation operators are spatial derivative operators in the direction of motion. For example, a horizontal translation operator is a derivative operator in the horizontal direction while a rotation operator computes a derivative circularly. Our

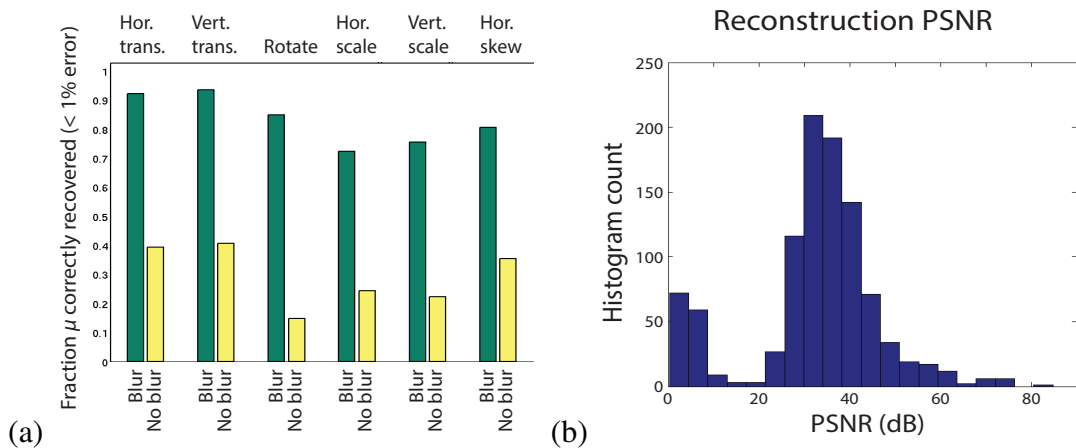


Figure 2: Performance in inferring transformation coefficients. (a) The fraction of recovered coefficients which differed by less than 1% from the true coefficient values. Image patches were transformed using a set of hand coded affine transformations (all transformations simultaneously), and recovery was performed via gradient descent of Equation 15. Inference with (“blur”) and without (“no blur”) adaptive smoothing is compared. (b) The distribution of PSNR values for image patches reconstructed using coefficients inferred with adaptive smoothing. The majority of transformed image patches are reconstructed with high PSNR.

learned operators exhibit this property. Figure 3 shows two of the learned transformation operators, where each 11×11 block corresponds to one column of A and the block’s position in the figure corresponds to its pixel location in the original image patch. This can be viewed as an array of basis functions, each one showing how intensity at a given pixel location influences the instantaneous change in pixel intensity at all pixel locations (see Equation 1). In this figure, each basis has become a spatial differentiator. The bottom two rows of Figure 3 show each of the operators being applied to an image patch. An animation of the full set of learned affine operators applied to image patches can be found at <http://redwood.berkeley.edu/jwang/affine.html> and in the supplemental material.

3.3 Learning Transformations from Natural Movies

To explore the transformation statistics of natural images, we trained the algorithm on pairs of 17×17 pixel image patches cropped from consecutive frames from the same video dataset as in Sections 3.1 and 3.2. In order to allow the learned transformations to capture image features moving into and out of a patch from the surround, and to allow more direct comparison to motion compensation algorithms, the error function for inference and learning was only applied to the central 9×9 region in each 17×17 patch. Each patch can therefore be viewed as a 9×9 patch surrounded by a 4 pixel wide buffer region. In the 15 transformation case a 2 pixel wide buffer region was used for computational reasons, so the 15 transformation case acts on 13×13 pixel patches with the reconstruction penalty applied on the central 9×9 region. Initialization was the same as in Section 3.1.

Training was performed on a variety of models with different numbers of transformations. For several of the models two of the operators were pre-specified to be whole-patch horizontal and vertical translation. This was done since we expect that translation will be the predominant mode of transformation in natural video, and this allows the algorithm to focus on learning less obvious transformations contained in video with the remaining operators. This belief is supported by the observation that several operators converge to full field translation when learning is unconstrained, as illustrated by the operator in Figure 4a from the 15 transformation case. Prespecifying translation also

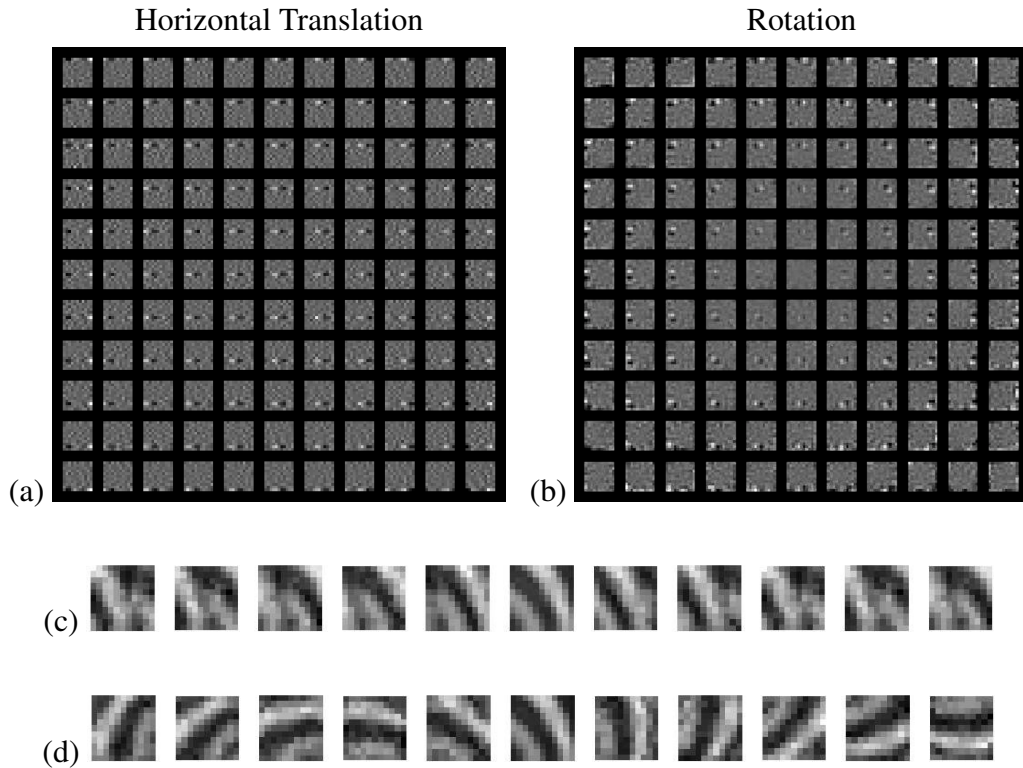


Figure 3: The learned transformation operators that corresponds to horizontal translation (*a*) and rotation (*b*). Each 11×11 block corresponds to one column of A and the block's position in the figure corresponds to its pixel location in the original image patch. Each block therefore shows how intensity at one pixel location contributes to the instantaneous change in intensity at all other pixel locations. Note that the blocks correspond to spatial derivatives in the direction of motion. Panels (*c*) and (*d*) show the translation and rotation operators, respectively, being applied to an image patch.

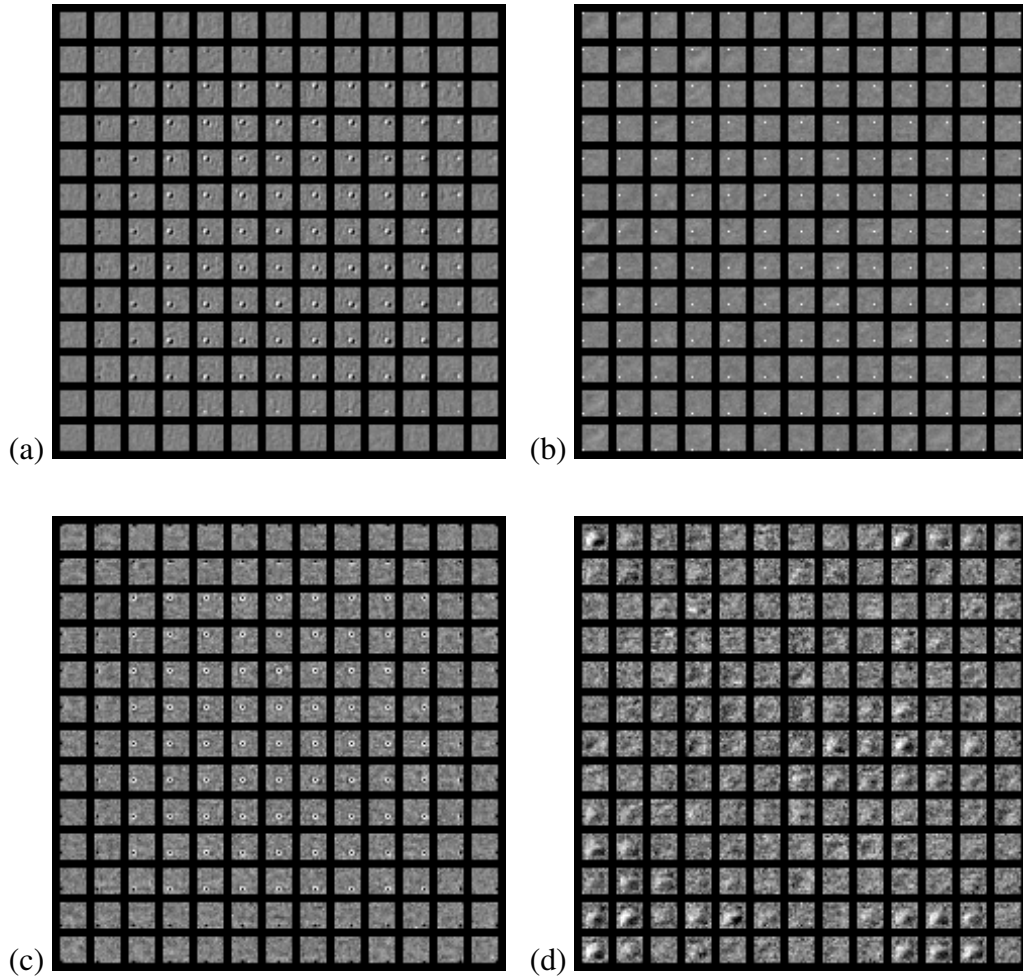


Figure 4: Sample transformation operators from a set of 15 transformations trained in an unsupervised fashion on 13×13 pixel patches (including a 2 pixel wide buffer region) from natural video. Each 13×13 block corresponds to one column of A and the block's position in the figure corresponds to its pixel location in the original image patch. Each block therefore illustrates the influence a single pixel has on the entire image patch as the transformation is applied. (a) full field translation operator, (b) full field intensity scaling, (c) full field contrast scaling, (d) unknown or difficult to interpret.

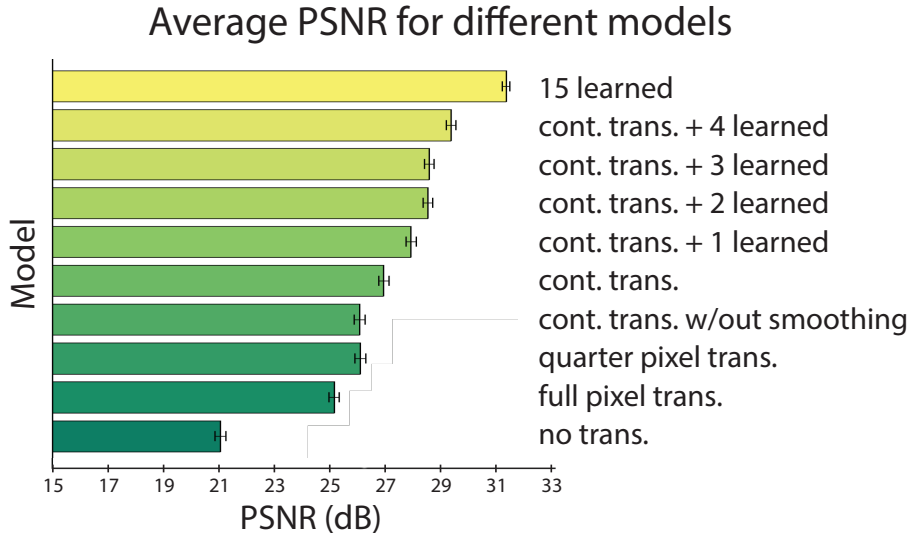


Figure 5: More complex models allow for more accurate representation of inter-frame differences. Bars show the PSNR of the reconstruction of a second frame via transformation of a first frame averaged over 1,000 pairs of frames from natural video, for a variety of model configurations.

provides a useful basis for comparing to existing motion compensation algorithms used in video compression, which are based on whole-patch translation.

The model case with the greatest variety of transformation operators consisted of 15 unconstrained transformations. A selection of the learned \mathbf{A}_k is shown in Figure 4. The learned transformation operators performed full field translations, intensity scaling, contrast scaling, spatially localized mixtures of the preceding 3 transformation types, and a number of transformations with no clear interpretation.

To demonstrate the effectiveness of the learned transformations at capturing the interframe changes in natural video, the PSNR of the image reconstruction for 1,000 pairs of 17×17 image patches extracted from consecutive frames was compared for all of the learned transformation models, as well as to standard motion compensation reconstructions. The models compared were as follows:

1. No transformation. Frame $\mathbf{x}^{(t)}$ is compared to frame $\mathbf{x}^{(t+1)}$ without any transformation.
2. Full pixel motion compensation. The central 9×9 region of $\mathbf{x}^{(t+1)}$ is compared

to the best matching 9×9 region in $\mathbf{x}^{(t)}$ with full pixel resolution.

3. Quarter pixel motion compensation with bilinear interpolation. The central 9×9 region of $\mathbf{x}^{(t+1)}$ is compared to the best matching 9×9 region in $\mathbf{x}^{(t)}$ with quarter pixel resolution.
4. Continuous translation without smoothing. Only vertical and horizontal translation operators are used in the model, but they are allowed to perform subpixel translations.
5. Continuous translation. Vertical and horizontal translation operators are used in the model, and in addition adaptive smoothing is used.
6. Continuous translation plus learned operators. Additional transformation operators are randomly initialized and learned in an unsupervised fashion.
7. 15 learned transformation operators. Fifteen operators are randomly initialized and learned in an unsupervised fashion. No operators are hard coded to translation.

As shown in Figure 5 there is a steady increase in PSNR as the transformation models become more complex. This suggests that as operators are added to the model they are learning transformations that are matched to progressively more complex frame-to-frame changes occurring in natural movies. Note also that continuous translation with adaptive smoothing yields a substantial improvement over quarter pixel translation. This suggests that the addition of a smoothing operator itself could be useful even when employed with the standard motion compensation model.

4 Discussion

We have described and tested a method for learning Lie group operators from high dimensional time series data, specifically image sequences extracted from natural movies. This builds on previous work using Lie group operators to represent image transformations by making four key contributions: 1) an eigen-decomposition of the Lie group operator, which allows for computationally tractable learning; 2) an adaptive smoothing operator that reduces local minima during inference; 3) a mechanism for combining

multiple non-commuting transformation operators; and 4) a method for regularizing coefficients by manifold distance traversed. The results obtained from both inferring transformation coefficients and learning operators from natural movies demonstrate the effectiveness of this method for representing transformations in complex, high-dimensional data.

In contrast to traditional video coding which uses a translation-based motion compensation algorithm, our method attempts to learn an optimal representation of image transformations from the statistics of the image sequences. The resulting model discovers additional transformations (beyond simple translation) to code natural video, yielding substantial improvements in frame prediction and reconstruction. The transformations learned on natural video include intensity scaling, contrast scaling, and spatially localized affine transformations, as well as full field translation.

The improved coding of inter-frame differences in natural video points to the potential utility of this algorithm for video compression. For this purpose the additional cost of encoding the transformation coefficients (μ and σ) needs to be accounted for and weighed against the gains in PSNR of the predicted frame. This tradeoff between encoding and reconstruction cost is explored, and a rate-distortion analysis performed, in a separate paper [Wang et al., 2011].

Beyond video coding, the Lie group method could also be used to represent complex motion in natural movies for the purpose of neurophysiological or psychophysical experiments. For example, neural responses could be correlated against the values of the inferred coefficients of the transformation operators. Alternatively, synthetic video sequences could be generated using the learned transformations, and the sensitivity of neural responses, or an observer, could be measured with respect to changes in the transformation coefficients. In this way, the learned transformation operators could provide a more natural set of features for probing the representation of transformations in the brain.

Another extension of this method would be to learn the transformations in a latent variable representation of the image, rather than directly on pixels. For example, one might first learn a dictionary to describe images using sparse coding [Olshausen and Field, 1996], and then model transformations among the sparse coefficients in response to a natural movie. Alternatively, one might infer a 3D model from the 2D image and

then learn the operators underlying the 3D transformations of objects in the environment, following the approach of [Bregler and Malik, 1998].

References

D.W. Arathorn. Map-seeking circuits in visual cognition: a computational mechanism for biological and machine vision. 2002.

M. J. Black and A. D. Jepson. Eigentracking: Robust matching and tracking of articulated objects using a view-based representation. *Proc. of the Fourth European Conference on Computer Vision*, pages 320–342, 1996.

Christoph Bregler and Jitendra Malik. Tracking people with twists and exponential maps. In *Computer Vision and Pattern Recognition, 1998. Proceedings. 1998 IEEE Computer Society Conference on*, pages 8–15. IEEE, 1998.

Taco Cohen and Max Welling. Learning the irreducible representations of commutative lie groups. *International Conference on Machine Learning*, 2014.

B.J. Culpepper and B.A. Olshausen. Learning transport operators for image manifolds. *Proceedings of Neural Information Processing Systems 22*, 2010.

E. Kokiopoulou and P. Frossard. Minimum distance between pattern transformation manifolds: Algorithm and applications. *IEEE Transactions on Pattern Analysis and Machine Intelligence*, 31(7):1225–1238, 2009.

M.S. Lewicki and B.A. Olshausen. Probabilistic framework for the adaptation and comparison of image codes. *Journal of the Optical Society of America*, 16(7):1587–1601, 1999.

B.D. Lucas and T. Kanade. An iterative image registration technique with an application to stereo vision. *Proceedings of Imaging understanding workshop*, pages 121–130, 1981.

R Memisevic and G Hinton. Learning to represent spatial transformations with factored higher-order boltzmann machines. *Neural Computation*, Jan

2010. URL <http://www.mitpressjournals.org/doi/pdf/10.1162/neco.2010.01-09-953>.
- X. Miao and R.P.N. Rao. Learning the lie groups of visual invariance. *Neural Computation*, 19(10):2665–2693, 2007.
- H Mobahi, CL Zitnick, and Y Ma. Seeing through the blur. *Computer Vision and Pattern Recognition*, 2012. URL http://ieeexplore.ieee.org/xpls/abs_all.jsp?arnumber=6247869.
- BA Olshausen and David J Field. Emergence of simple-cell receptive field properties by learning a sparse code for natural images. *Nature*, 1996. URL http://redwood.psych.cornell.edu/papers/olshausen_field_nature_1996.pdf.
- B.A. Olshausen, C. Cadieu, B.J. Culpepper, and D. Warland. Bilinear models of natural images. *SPIE Proceedings vol. 6492: Human Vision Electronic Imaging XII (B.E. Rogowitz, T.N. Pappas, S.J. Daly, Eds.)*, 2007.
- M. Ortiz, R.A. Radovitzky, and E.A Repetto. The computation of the exponential and logarithmic mappings and their first and second linearizations. *International Journal For Numerical Methods In Engineering*, 52:1431–1441, 2001.
- R.P.N Rao and D.L. Ruderman. Learning lie groups for invariant visual perception. *Advances in Neural Information Processing Systems 11*, pages 810–816, 1999.
- Mark Schmidt. minfunc. Technical report, <http://www.cs.ubc.ca/~schmidtm/Software/minFunc.html>, 2009. URL <http://www.cs.ubc.ca/~schmidtm/Software/minFunc.html>.
- J. Shen. Resampling volume or image with affine matrix. <http://www.mathworks.com/matlabcentral/fileexchange/21080>, 2008.
- Evan C Smith and Michael S Lewicki. Efficient auditory coding. *Nature*, 439(7079): 978–982, 2006.

- J H van Hateren and A van der Schaaf. Independent Component Filters of Natural Images Compared with Simple Cells in Primary Visual Cortex. *Proceedings: Biological Sciences*, 265(1394):359–366, March 1998.
- N. Vasconcelos and A. Lippman. Multiresolution tangent distance for affine invariant classification. *Proceedings of Neural Information Processing Systems 10*, 1997.
- C.M. Wang, J. Sohl-Dickstein, I. Tasic, and B.A. Olshausen. Lie group transformation models for predictive video coding. *Data Compression Conference*, pages 83–92, 2011.
- W. Wiegand, G.J. Sullivan, G. Bjontegaard, and A. Luthra. Overview of the h.264/avc video coding standard. *IEEE Transactions on Circuits and Systems for Video Technology*, 13(7):560–576, 2003.

A Appendix - Degeneracy in U

We decompose our transformation generator

$$A = V\Lambda V^{-1} \tag{A-1}$$

where Λ is diagonal. We introduce another diagonal matrix R . The diagonal of R can be populated with any non-zero complex numbers, and the following equations will still hold:

$$A = V\Lambda V^{-1} \tag{A-2}$$

$$= VRR^{-1}\Lambda V^{-1} \tag{A-3}$$

$$= VR\Lambda R^{-1}V^{-1} \tag{A-4}$$

$$= (VR)\Lambda(VR)^{-1} \tag{A-5}$$

If we set

$$U = VR \tag{A-6}$$

then

$$A = U\Lambda U^{-1} \tag{A-7}$$

and R represents a degeneracy in U .

We remove this degeneracy in U by choosing R so as to minimize the joint power after every learning step. That is

$$R = \underset{R}{\operatorname{argmin}} \sum_i \sum_j V_{ij}^2 R_{jj}^2 + \sum_i \sum_j (R^{-1})_{jj}^2 (V^{-1})_{ji}^2 \quad (\text{A-8})$$

$$= \underset{R}{\operatorname{argmin}} \sum_i \sum_j V_{ij}^2 R_{jj}^2 + \sum_i \sum_j (V^{-1})_{ji}^2 \frac{1}{R_{jj}^2} \quad (\text{A-9})$$

setting the derivative to 0

$$2 \sum_i V_{ij}^2 R_{jj} - 2 \sum_i (V^{-1})_{ji}^2 \frac{1}{R_{jj}^3} = 0 \quad (\text{A-10})$$

$$R_{jj} \sum_i V_{ij}^2 = \frac{1}{R_{jj}^3} \sum_i (V^{-1})_{ji}^2 \quad (\text{A-11})$$

$$R_{jj}^4 = \frac{\sum_i (V^{-1})_{ji}^2}{\sum_i V_{ij}^2} \quad (\text{A-12})$$

$$R_{jj} = \left[\frac{\sum_i (V^{-1})_{ji}^2}{\sum_i V_{ij}^2} \right]^{\frac{1}{4}}. \quad (\text{A-13})$$

Practically this means that, after every learning step, we set

$$R_{jj} = \left[\frac{\sum_i (U^{-1})_{ji}^2}{\sum_i U_{ij}^2} \right]^{\frac{1}{4}} \quad (\text{A-14})$$

and then set

$$U_{new} = UR. \quad (\text{A-15})$$

B Appendix - Derivatives

Let

$$\varepsilon = \sum_n (Y_n - U e^{\mu\Lambda} e^{\frac{1}{2}\Lambda^2\sigma^2} U^{-1} X_n)^2 \quad (\text{B-1})$$

B.1 Derivative for inference with one operator

The learning gradient with respect to μ is

$$\begin{aligned} \frac{\partial \varepsilon}{\partial \mu} &= - \sum_n 2err(n) U \frac{\partial e^{\mu\Lambda}}{\partial \mu} e^{\frac{1}{2}\Lambda^2\sigma^2} U^{-1} X_n \\ &= - \sum_n 2err(n) U \Lambda e^{\mu\Lambda} e^{\frac{1}{2}\Lambda^2\sigma^2} U^{-1} X_n \end{aligned} \quad (\text{B-2})$$

where $err(n)$ is the reconstruction error of the n^{th} sample

$$err(n) = Y_n - Ue^{\mu\Lambda}e^{\frac{1}{2}\Lambda^2\sigma^2}U^{-1}X_n \quad (\text{B-3})$$

Similarly, the learning gradient with respect to σ is

$$\frac{\partial\varepsilon}{\partial\sigma} = -\sum_n 2err(n)Ue^{\mu\Lambda}\sigma\Lambda^2e^{\frac{1}{2}\Lambda^2\sigma^2}U^{-1}X_n \quad (\text{B-4})$$

B.2 Derivative for learning with one operator

The learning gradient with respect to Λ is

$$\begin{aligned} \frac{\partial\varepsilon}{\partial\Lambda} &= -\sum_n 2err(n)U\frac{\partial\left[e^{\mu\Lambda}e^{\frac{1}{2}\Lambda^2\sigma^2}\right]}{\partial\Lambda}U^{-1}X_n \\ &= -\sum_n 2err(n)U(\mu e^{\mu\Lambda} + \sigma^2\Lambda e^{\frac{1}{2}\Lambda^2\sigma^2})U^{-1}X_n \end{aligned} \quad (\text{B-5})$$

The learning gradient with respect to U is

$$\begin{aligned} \frac{\partial\varepsilon}{\partial U} &= -\sum_n 2err(n)\frac{\partial U}{\partial U}e^{\mu\Lambda}e^{\frac{1}{2}\Lambda^2\sigma^2}U^{-1}X_n \\ &\quad -\sum_n 2err(n)Ue^{\mu\Lambda}e^{\frac{1}{2}\Lambda^2\sigma^2}\frac{\partial U^{-1}}{\partial U}X_n \end{aligned} \quad (\text{B-6})$$

Recall that

$$\frac{dU^{-1}}{dU} = -U^{-1}\frac{dU}{dU}U^{-1}. \quad (\text{B-7})$$

The learning gradient is therefore

$$\begin{aligned} \frac{\partial\varepsilon}{\partial U} &= -\sum_n 2err(n)e^{\mu\Lambda}e^{\frac{1}{2}\Lambda^2\sigma^2}U^{-1}X_n \\ &\quad +\sum_n 2err(n)Ue^{\mu\Lambda}e^{\frac{1}{2}\Lambda^2\sigma^2}U^{-2}X_n \end{aligned} \quad (\text{B-8})$$

B.3 Derivative for Complex Variables

To accommodate for the complex variables U and Λ , we rewrite our objective function as

$$\varepsilon = \sum_n err(n)^T \overline{err(n)} \quad (\text{B-9})$$

where $\overline{err(n)}$ denotes the complex conjugate. The derivative of this error function with respect to any complex variable can be then broken into the derivative with respect to the real and and imaginary parts. This results in

$$\begin{aligned}\frac{\partial \varepsilon}{\partial \mathcal{R}\{\Lambda\}} &= 2\mathcal{R}\left\{\sum_n err(n)^T \overline{\left(\frac{\partial err(n)}{\partial \Lambda}\right)}\right\} \\ \frac{\partial \varepsilon}{\partial \mathcal{I}\{\Lambda\}} &= -2\mathcal{I}\left\{\sum_n err(n)^T \overline{\left(\frac{\partial err(n)}{\partial \Lambda}\right)}\right\},\end{aligned}\tag{B-10}$$

(similarly for U).

B.4 Derivatives for Manifold Penalty

We have a model

$$\dot{I} = AI\tag{B-11}$$

with solution

$$I_1 = e^{As} I_0.\tag{B-12}$$

We want to find and minimize the distance traveled by the image patch I_0 to I_1 under the transformation operator A . The total distance is

$$d = \int_{t=0}^s \|\dot{I}\|_2 dt.\tag{B-13}$$

This then gives the following,

$$\begin{aligned}d &= \int_{t=0}^s \|Ax^{(t)}\|_2 dt \\ &= \int_{t=0}^s \|Ae^{At} I_0\|_2 dt \\ &= \int_{t=0}^s \sqrt{(Ae^{At} I_0)^T (Ae^{At} I_0)} dt \\ &= \int_{t=0}^s \sqrt{I_0^T (e^{At})^T A^T A e^{At} I_0} dt.\end{aligned}\tag{B-14}$$

We don't know how to solve this analytically. Instead we make the approximation

$$\begin{aligned}\int_{t=0}^s \|\dot{I}\|_2 dt &\approx |s| \|AI_{\frac{s}{2}}\|_2 \\ &= |s| \|Ae^{A\frac{s}{2}} I_0\|_2,\end{aligned}\tag{B-15}$$

with derivative

$$\frac{\partial}{\partial s} [|s| \|Ae^{A\frac{s}{2}} I_0\|_2] = B + 2sB,\tag{B-16}$$

where $B = I_0^T (e^{A\frac{s}{2}})^T A^T A e^{A\frac{s}{2}} I_0$